Numerical Investigation of Pressure Load over Spillway Chutes with Vertical Curvatures

SAEED-REZA SABBAGH-YAZDI*, FATEMEH ROSTAMI**
Civil Engineering Department,
KN Toosi University of Technology,
No.1346 Valiasr Street, 19697- Tehran, IRAN

and
NIKOS E. MASTORAKIS
Military Insitutes of University Education (ASEI)
Hellenic Naval Academy
Terma Chatzikyriakou 18539,
Piraues, GREECE

Abstract: For flow conduits with mild slope and considerably large vertical curvatures the hydrostatic distribution of the pressure may be used for design proposes. However, for the spillway chutes actual pressure load over the steep slope beds with small vertical curvatures may differ from the hydrostatic pressure values. The differences in pressure load on curved bed chutes are mainly because of the centrifugal forces. In present work a two dimensional Finite Volume flow solver, which utilizes the Volume of Fluid technique, is devised to investigate the division of the numerically computed pressure from the hydrostatic assumptions using some measurements for laboratory test cases reported in the literature.

Key-Words: Numerical Simulations, Non-hydrostatic pressure, Curved bed, Volume of Fluid (VOF).

1 Introduction

Rapidly varied transitions in open channels typically involve flows with high curvatures and or slop. The length of such transition is usually short and pressure distribution significantly non-hydrostatics and velocity distributions are highly non-uniform.

At present most computational modeling of open channel flows are based on the depth-averaged St. Venant equations, in these equations, a uniform longitudinal velocity and hydrostatic pressure distribution are assumed. Correction coefficients may be applied for different distributions if they can be established a priori (Yen 1973). These equations are applicable for very shallow flows, with wavelength-to-depth ratios in excess of about 20 (Henderson 1966). For moderately shallow flows (i.e., for shorter feature wavelengths), the Boussinesq equation are the next level of approximation (Chaudhry 1993). While the Boussinesq equation are applicable to some what shorter lengths (about six depths), they do not appear to have been successfully applied to problems whit steep slopes (Montes 1994).

Dressler (1978) attempt to extend the one dimensional approach to higher- curvature flows by using a curvilinear, orthogonal coordinate system based on the bed geometry. This approach, applied by Sivakumaran et al. (1983), is based on a potential-flow assumption. The method, how ever dose not account for the water-surface curvature being different from the bed curvature being different from the bed curvature and reduces to the St. Venant equation for a flat bed.

Hager and Hutter (1984) presented the method, based on potential flow in a streamline coordinate system, which assumes a linear variation of flow angle and curvature between the bed and surface. The result was shown to be an improvement over the Boussinesq equation but limited to geometrically mild slopes (up to about 60°). A similar but higher-order method was developed by Matthew (1991) in Cartesian coordinate system. This method involves an iterative solution. Corrections for the effect of friction were also incorporated.

A further alternative was presented by Steffler and Jin (1993). There, the plane Reynolds equation were vertically averaged, and moment equations were developed by vertically integrating the Reynolds equations after they had been multiplied by vertical coordinate, The three extra equations allow specification of three further flow parameters. Linear longitudinal velocities as well as quadratic-

pressure and vertical-velocity distributions were assumed, and equations were rewritten in terms of parameters of these distributions. Essentially, the approach amounts to a low-order weighted residual method. The method suffers from the crudeness and arbitrariness of the assumed distributions, and results in some long and complex equations where the terms are not of uniform order. It does have the advantage of incorporating the effect of turbulent stresses directly, although these are not important in the applications considered in this paper.

In this paper, a module of ***FLOW-3D***® flow solver which uses first order finite volume scheme for structured meshes is applied to model the free surface flow over the two small scale test cases. First, flow from horizontal to a steep slope whit a circular arc transition is modeled. Second, flow over a symmetric and an asymmetric bed profile is tested. Note that, the utilized software applies the True-VOF (volume-of-fluid) technique for treatment of the free surface, and hence, dose not incorporates any hydrostatic pressure distribution assumption (i.e. "streamline curvature" explicit consideration).

2 Governing equation

The general mass continuity equation is:

$$V_f \frac{\partial \rho}{\partial t} + \frac{\partial}{\partial x}(\rho u A_x) + \frac{\partial}{\partial z}(\rho w A_z) = 0 \qquad (1)$$

Where V_f is the fractional volume open to flow, ρ is the fluid density. The velocity components (u,w) are in the coordinate directions (x,z). A_y and A_z are similar area fractions for flow in the y and z directions, respectively.

The equation of motion for the fluid velocity components in the two directions are the Navier – Stokes equations as follows:

$$\frac{\partial u}{\partial t} + \frac{l}{V_f}\left\{uA_x\frac{\partial u}{\partial x} + wA_z\frac{\partial u}{\partial z}\right\} = -\frac{l}{\rho}\frac{\partial p}{\partial x} + G_x + f_x \qquad (2)$$

$$\frac{\partial w}{\partial t} + \frac{l}{V_f}\left\{uA_x\frac{\partial w}{\partial x} + wA_z\frac{\partial w}{\partial z}\right\} = -\frac{l}{\rho}\frac{\partial p}{\partial z} + G_z + f_z \qquad (3)$$

In these equations G_x, G_z are body accelerations, and f_x, f_z are viscous accelerations that for a variable dynamic viscosity μ are as follows:

$$\rho V_f f_x = -\left\{\frac{\partial}{\partial x}(A_x\tau_{xx}) + \frac{\partial}{\partial z}(A_z\tau_{xz})\right\} \qquad (4)$$

$$\rho V_f f_z = -\left\{\frac{\partial}{\partial x}(A_x\tau_{xz}) + \frac{\partial}{\partial z}(A_z\tau_{zz})\right\} \qquad (5)$$

Where:

$$\tau_{xx} = -2\mu\frac{\partial u}{\partial x} \qquad (6)$$

$$\tau_{zz} = -2\mu\frac{\partial w}{\partial z} \qquad (7)$$

$$\tau_{xz} = -\mu\left\{\frac{\partial u}{\partial z} + \frac{\partial w}{\partial x}\right\} \qquad (8)$$

$$\tau_{yz} = -\mu\left\{\frac{\partial v}{\partial z} + \frac{\partial w}{\partial y}\right\} \qquad (9)$$

Fluid configuration is defined in terms of a volume of fluid (VOF) function, F(x, z, and t). This function represents the volume of fluid per unit volume and satisfies the equation.

$$\frac{\partial F}{\partial t} + \frac{l}{V_F}\left[\frac{\partial}{\partial x}(FA_x u) + \frac{\partial}{\partial z}(FA_z w)\right] = \circ \qquad (10)$$

The interpretation of F depends on the type of problem being soled. For a single fluid, F represents the volume fraction occupied by the fluid. Thus fluid exists where F=1 and void regions correspond to locations where F=0. Voids are regions without fluid mass that have a uniform pressure assigned to them. Physically they represent regions filled with a vapor or gas whose density is insignificant with respect to fluid density.

3 Numerical Simulation

FLOW-3D® numerically solves the equations described in the previous sections using finite-difference (or finite-volume) approximations. The flow region is subdivided into a mesh of fixed rectangular cells. With each cell there are associated local average values of all dependent variables. All variables are located at the centers of the cells except for velocities, which are located at cell faces (staggered grid arrangement). [1]

Curved obstacles, wall boundaries, or other geometric features are embedded in the mesh by defining the fractional face areas and fractional volumes of the cells that are open to flow (the FAVOR™ method).[1]

Pressures and velocities are coupled implicitly by using time-advanced pressures in the momentum equations and time-advanced velocities in the mass (continuity) equation. This semi-implicit formulation of the finite-difference equations allows for the efficient solution of low speed and incompressible flow problems. The semi-implicit formulation, however, results in coupled sets of equations that must be solved by an iterative technique. In ***FLOW-3D***® two such techniques are provided. The

simplest is a successive over-relaxation (SOR) method. In some instances, where a more implicit solution method is required, a special alternating-direction, line-implicit method (SADI) is available. The SADI technique can be used in one, two, or in all three directions depending on the characteristics of the problem to be solved.

The basic numerical method used in ***FLOW-3D***® has a formal accuracy that is first order with respect to time and space increments. Special precautions have been taken to maintain this degree of accuracy even when the finite-difference mesh is non-uniform.

A new VOF advection method based on a 3-D reconstruction of the fluid interface has been developed and implemented in ***FLOW-3D***® Version 8.2. The Volume-of-Fluid (VOF) function is moved in one step, without resorting to an operator splitting technique, which gives the present method increased accuracy when the flow is not aligned with a coordinate direction.

The existing VOF advection method in FLOW-3D® is based on the donor-acceptor approach first introduced by Hirt and Nichols.

3.1 Transition from horizontal to steep slop

For this part of numerical investigation, the experimental measurements reported by Montes (1994) are used. The experimental data for water-surface and bed pressure profiles obtained from the plots provided by Montes (1994). These experiments were performed in a smooth channel 0.402 m wide. The steep slope 45° was studied. For this slop transition from horizontal to steep slop was obtained trough a circular arc of 0.1-m radius.

The model boundary condition for this case, with critical flow occurring at upstream boundary, are specified upstream depth (h_0) and vanishing derivatives of extra pressure and velocity variables. As downstream flow is supercritical, no conditions are applied at downstream end. For this case the bed shear stress term in neglected.

Figs. 1 and 3 show the compute velocity magnitude and pressure couture and Figs. 2 and 4 show the compute and measured water-surface and bed-pressure profiles for different discharges. The model predicted both the water-surface and bed-pressure extremely well. The agreement appears to improve with increasing discharge.

The hydrostatic bed-pressure also shows in Fig. 3. The computed pressure distribution presents little differences with hydrostatic pressure distribution except for transition sections. These differences are due to curved bed in transition and efficiency of centrifugal acceleration.

3.2 Symmetric and Asymmetric bed profiles

The experimental measurements reported by Sivakumaran et al. (1983) are used for the present numerical investigation. These experiments were performed in a horizontal flume 915 cm long, 65 cm high and 30 cm wide. Two symmetric and asymmetric bed profiles, as shown in Figs. 5 and 9 were tested. The leading edge of profile in each case was placed 366 cm downstream from the inlet box, i.e., head tank. The upstream undisturbed depth was measured at 16 cm from leading edge of profile. The symmetric profile was shaped according to a normal distribution, and was 20 cm high and 120 cm long. The asymmetric profile, with a 150-cm length, was achieved by passing a B-spline through a fixed set of coordinates. Further details of experimental system and bed profile can be found in Sivakumaran and et al. (1983).

The results of model along with experimental data for the symmetric are shown in Figs. 6 and 8. For the low flow, the predicted water-surface elevation matches well with the measured data in the supercritical region, while the results in sub-critical regions follow the hydrostatic pressure distributions. The modeled bed pressures compare well with the measured data in the sub-critical region, while in the supercritical region the measured data show some scatter that is due to local turbulence resulting from bed curvature, as discussed by Sivakumaran et al. (1983). The pressure deviated from hydrostatic pressure distribution in the high curvature zone and this gap increases for high flow rate. For the high flow rate, the predicted water-surface elevation matches well with the measured data in the supercritical region. For the supercritical region, the model predicts a lower water surface elevation and bed pressure, while oscillations are predicted for both surface elevation and bed pressure just upstream from the crest.

The results for the asymmetric shape are shown in Figs. 9-12. For the asymmetric shape, Figs. 10 and 12 show the compute and measured water-surface and bed-pressure profiles for various discharges. The predicted depth and pressure in region of steep slope matches well with measured data if the bed and water surface curvatures are considerably large. However, for higher flow rate the numerical results present better agreements with experimental measurements in the steep slope regions.

4 Conclusion

The results of present numerical investigations show that the predicted water-surface elevation matches well with the measured data. The computed pressures by the utilized three-dimensional flow solver (which uses True-VOF technique for computation of water free surface) are in good agreements with the experimental measurements. However, the computed the pressures at the bottom surface of chutes with vertical curvatures slightly differ from the measured pressure in some parts of the super-critical flow parts. The computed pressures along the conduit differ from the hydrostatic assumption due to curved bed and efficiency of centrifugal acceleration. The differences are more pronounce at the zones with considerably large vertical curvatures, particularly for high flow rates. Therefore, it can be stated that, in the regions with large bottom curvature the pressure distribution does not follow the hydrostatic pressure profile. For the convex bottom curvature the hydrostatic assumption for pressure is more than the actual pressure, while in concave curvature the contrary condition is observed.

References:

[1] ***FLOW-3D®*** user manual, Ver. 8.2

[2] C.W. Hirt and B.D. Nichols, "Volume of Fluid (VOF) Method for the Dynamics of Free Boundaries", *J. Comp. Phys.*, Vol. 39, 1981, pp.201-225.

[3] Abdul A. Khan, Peter M. Steffler. "Vertically Averaged and Moment Equation Model for Flow over Curved Beds." *Journal of Hydraulic Engineering*, Vol.122, No. 1,1996.

[4] Montes, J. S. "Potential-flow solution to 2D transition from mild to steep slop." *Journal of Hydraulic Engineering*, ASCE, Vol. 1(5), 1994, pp. 601-621.

[5] Sivakumaran, N. S., Tingsanchali, T., and Hosking, R. J. "Steady shallow flow over curved beds." *J. Fluid Mech.,*Vol. 128, 1983, pp. 469-487.

[6] Chow, V. T., *Open-Channel Hydraulics*, Mc.Grow Hill Book, PP.444-448, 1973.

[7] Chaudhry, R. F. *Open channel flow*, Precentice-Hall, Englewood Cliffs, N.J. 1993.

[8] Dressler, R. F. () "New nonlinear shallow-flow equations with curvature." *J. Hydr. Res*., Vol. 16, No. 3, 1978, pp. 205-220.

[9] Gharangik, A. M., and Chaudry, M. H. "Numerical simulation of hydraulic jump." *J. Hydr. Engrg., ASCE*, Vol. 117, No. 9, pp. 1195-1211.

[10] Hager, W. H. "Equation for moderately curved open channel flow." *J. Hydr. Engrg., ASCE*, Vol. 111, No. 3, pp. 541-546.

[11] Hager, W.H., and Hutter, K. "Approximate treatment of paln channel flow." *Acta Mechanica*, Vol. 51, pp. 21-48.

[12] Henderson,F. *Open channel flow.* Macmilian, New York, N.Y.1966.

[13] Hicks, F. E., and Steffler, P. M. "Characteristic dissipative Galerkin scheme for open-channel flow" *J. Hydr. Engrg., ASCE*, Vol. 118, No. 2, 1992. pp. 337-352.

[14] Matthew, G. D. "higher order one-dimensional equations of potential flow in open channels." *Proc., Institution of Civil Engineers. London, Englad*, Vol. 2(91), 1991, pp. 187-201.

[15] Rao, N. S. L. "Theory of weirs." *Advance in hydroscience,* Vol. 10, 1975.

[16] Steffler, P. M. and Jin, Y. "Depth averaged and moment equations for moderately shallow free surface flow." *J. Hydr. Res*., Vol. 31, No. 1, 1993,pp. 5-17.

[17] Yen, B. C. "Open channel flow equations revisited." *J. Engrg. Mech. Div. ASCE*, Vol. 99, No. 5, 1973. pp. 99-1009.

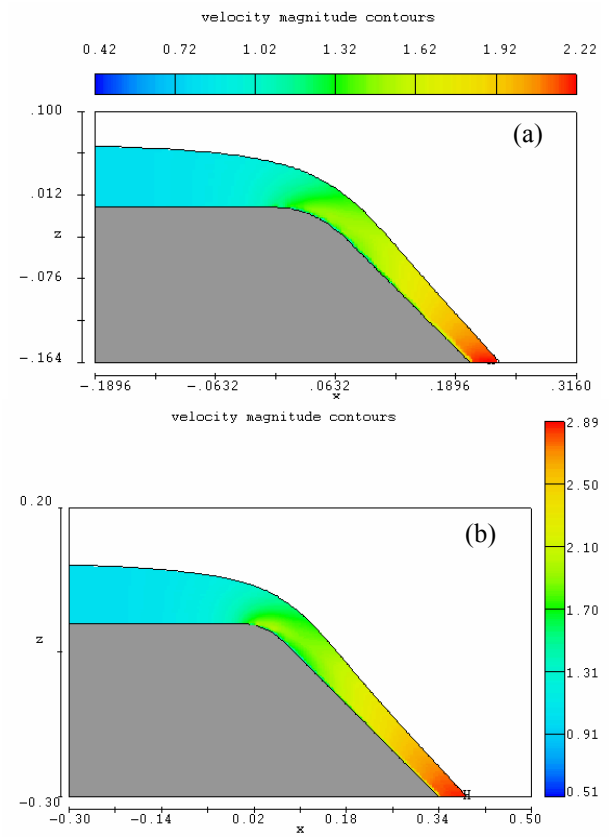

Fig. 1, Computed velocity magnitude contours (m/s) for 45° slop: (a) Q=0.02 m^3/s; (b) Q=0.04 m^3/s.

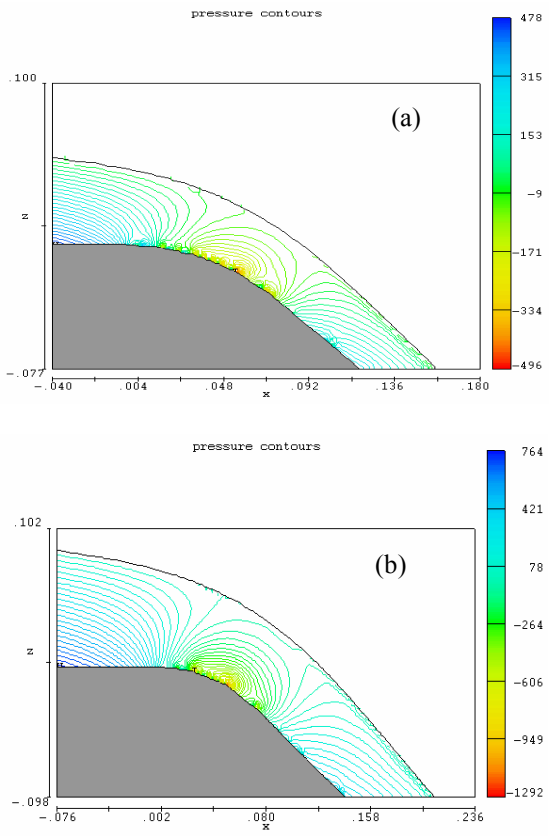

Fig. 3, Computed pressure contours (Pa) for transition 45° slop: (a) Q=0.02 m^3/s; (b) Q=0.04 m^3/s.

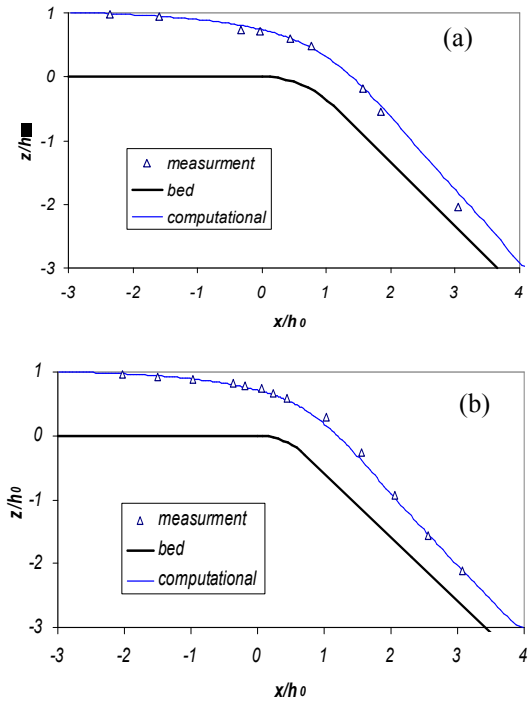

Fig. 2, Water-Surface profile for transition 45° slop: (a) Q=0.02 m^3/s; (b) Q=0.04 m^3/s.

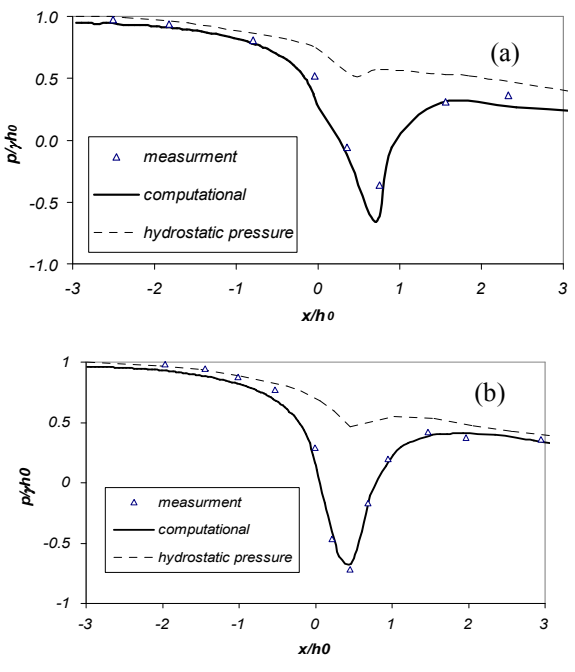

Fig. 4, Bed-Pressure for transition 45° slop: (a) Q=0.02 m^3/s; (b) Q=0.04 m^3/s.

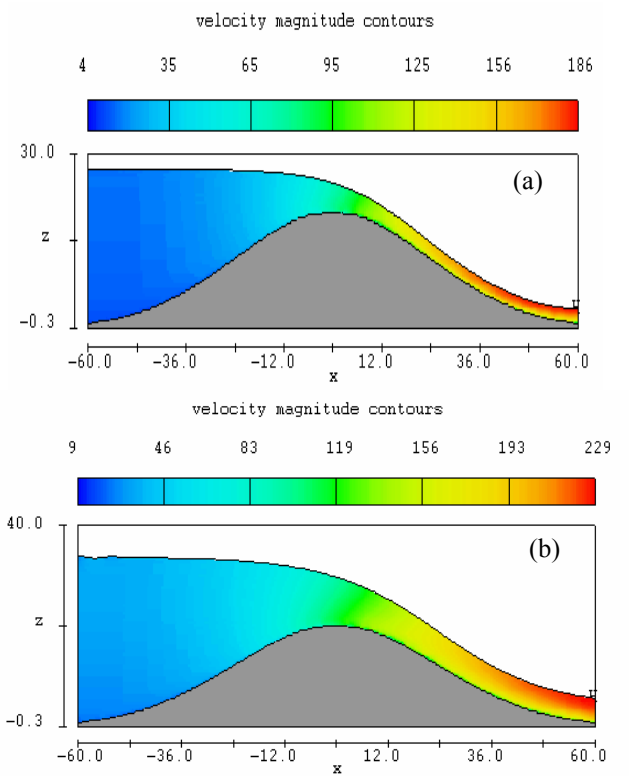

Fig. 5, Computed velocity magnitude (m/s) for symmetric bed form
(a) q=359.9 m^2/s, (b) q=1,119.7 m^2/s.

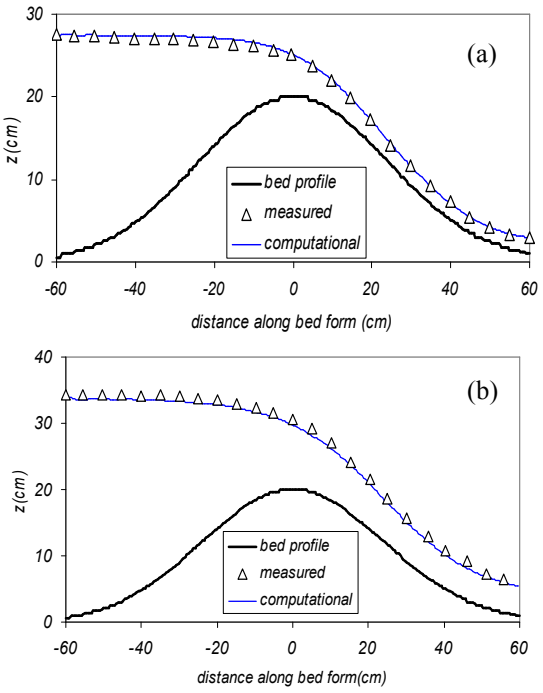

Fig. 6, Water-Surface profile for symmetric bed form:
(a) q=359.9 m^2/s, (b) q=1,119.7 m^2/s.

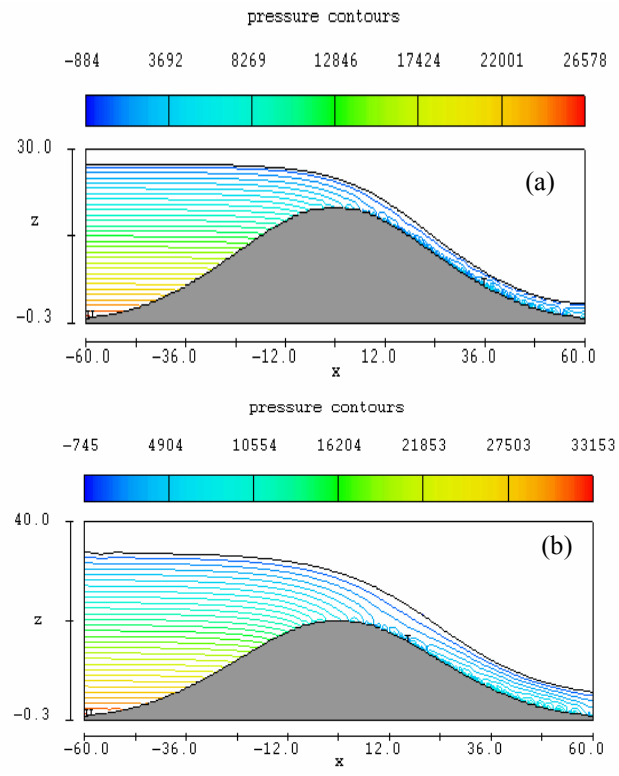

Fig. 7, Computed pressure contours (Pa) for symmetric bed
(a) q=359.9 m^2/s, (b) q=1,119.7 m^2/s.

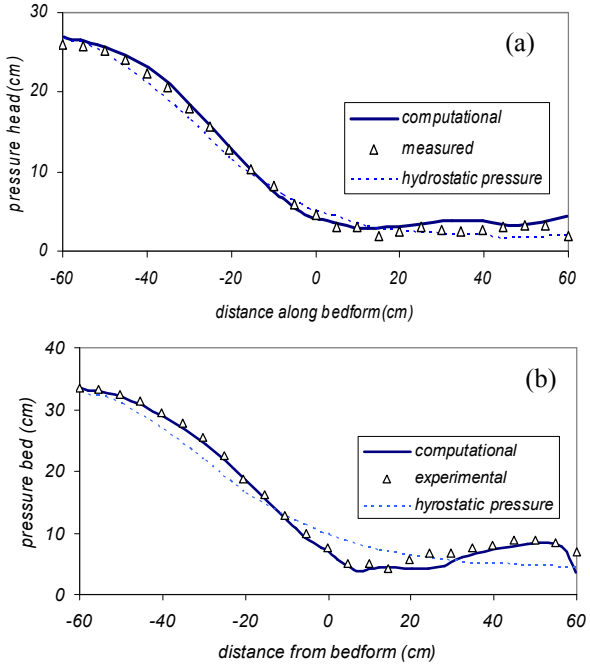

Fig. 8, Bed-Pressure for symmetric bed form:
(a) q=359.9 m^2/s, (b) q=1,119.7 m^2/s.

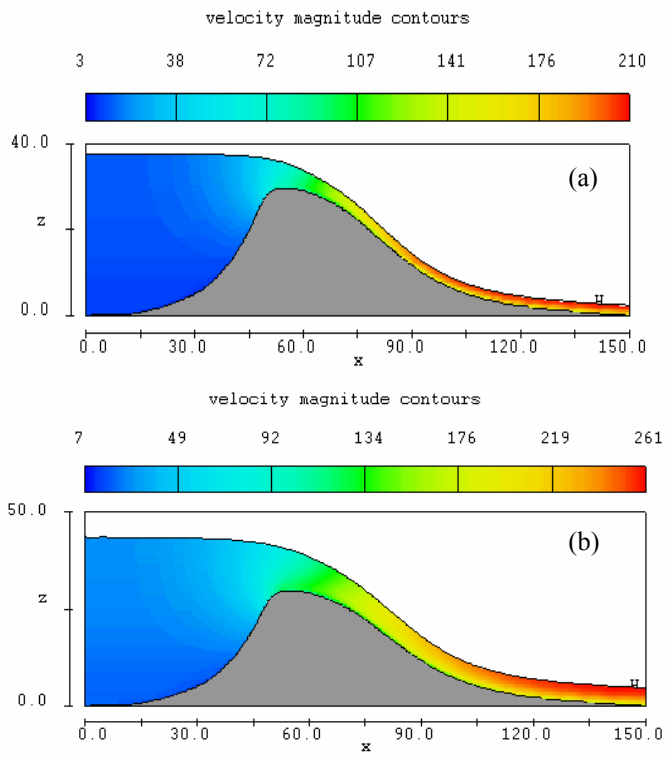

Fig. 9, Computed velocity magnitude (m/s) for asymmetric bed form: (a) q=375.0 m^2/s, (b) q=1,116.5 m^2/s.

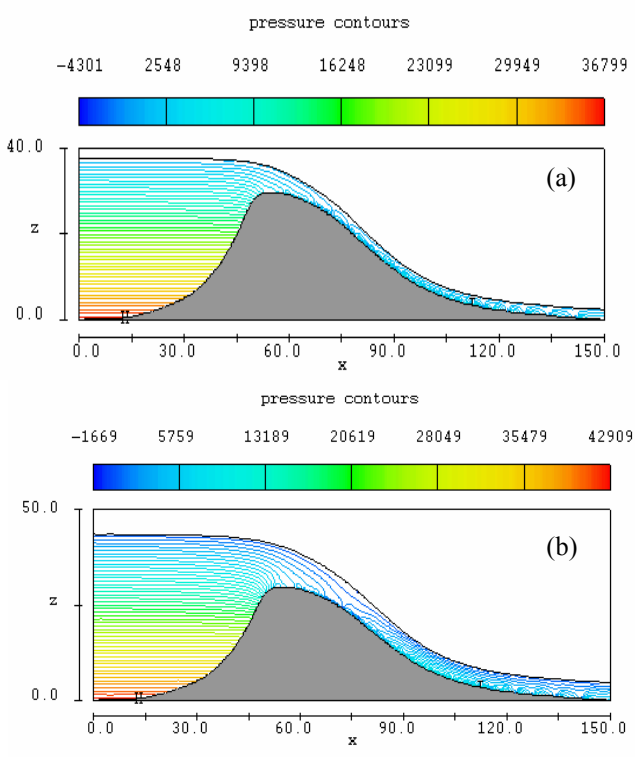

Fig. 11, Computed pressure contour (Pa) for asymmetric bed form: (a) q=375.0 m^2/s, (b) q=1,116.5 m^2/s.

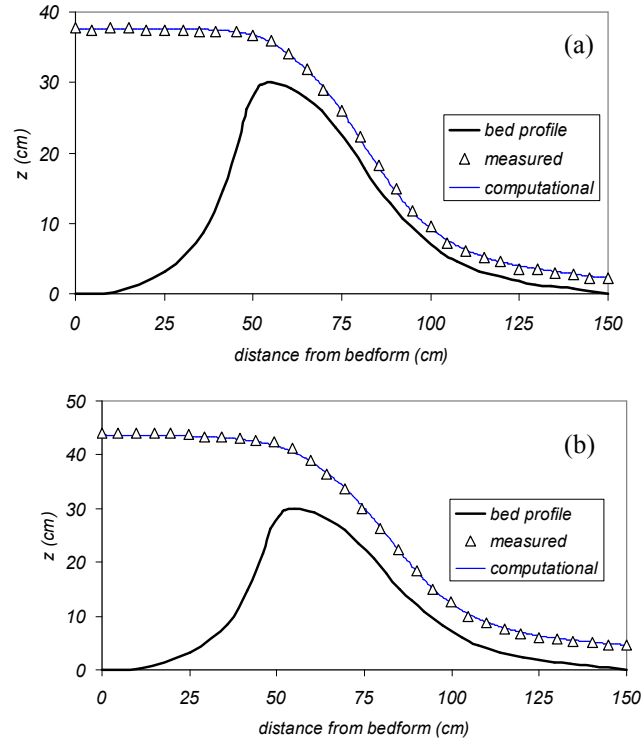

Fig. 10, Water-Surface profile for asymmetric bed form: (a) q=375.0 m^2/s, (b) q=1,116.5 m^2/s.

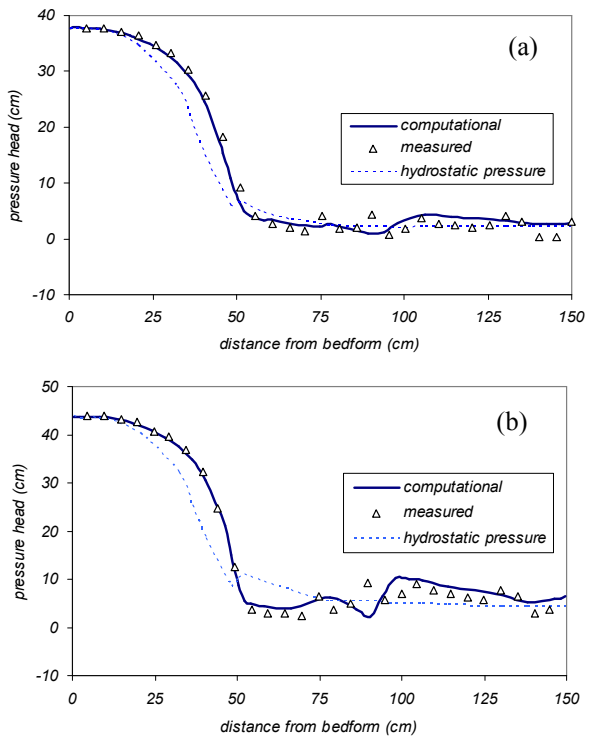

Fig. 12, Bed-Pressure for asymmetric bed form: (a) q=375.0 m^2/s, (b) q=1,116.5 m^2/s.